

Modeling of Combined Impact and Blast Loading on Reinforced Concrete Slabs

Abstract

Explosive devices represent a significant threat to military and civilian structures. Specific design procedures have to be followed to account for this and ensure buildings will have the capacity to resist the imposed pressures. Shrapnel can also be produced during explosions and the resulting impacts can weaken the structure, reducing its capacity to resist the blast pressure wave and potentially causing failures to occur. Experiments were performed by the Defence Science and Technology Agency (DSTA) of Singapore to study this combined loading phenomenon. Slabs were placed on the ground and loaded with approximately 9 kg TNT charges at a standoff distance of 2.1 m. Spherical steel ball bearings were used to reproduce the shrapnel loading. Loading and damage characteristics were recorded from the experiments. A finite element analysis (FEA) model was then created which could simulate the effect of combined shrapnel impacts and blast pressure waves in reinforced concrete slabs, so that its results could be compared to experimental data from the blast tests. Quarter models of the experimental concrete slabs were built using LS-Dyna. Material models available in the software were employed to represent all the main components, taking into account projectile deformations. The penetration depth and damage areas measured were then compared to the experimental data and an analytical solution to validate the models.

Keywords

Blast, impact, concrete, FEA

P. Del Linz ^a

S.C. Fan ^b

C.K. Lee ^c

^a School of Civil and Environmental Engineering, Nanyang Technological University, Nanyang Avenue, 639798 Singapore. Email: paolo@ntu.edu.sg

^b School of Civil and Environmental Engineering, Nanyang Technological University, Nanyang Avenue, 639798 Singapore. Email: cfansc@ntu.edu.sg

^c School of Engineering and Information Technology, The University of New South Wales, Canberra, Australia. Email: c.lee@adfa.edu.au

<http://dx.doi.org/10.1590/1679-78252516>

Received 06.10.2015

In revised form 14.03.2016

Accepted 08.04.2016

Available online 12.04.2016

1 INTRODUCTION

Very low stand-off explosions of real ammunition can produce significant amounts of shrapnel, which will be propelled at high velocities onto structures. The impact of these fragments can repre-

sent a significant loading for structural elements and its effects will be compounded to the damage caused by the blast shock wave (Hader, 1983; Nyström and Gylltoft, 2009). Therefore, designing structures to resist low stand-off blast loads requires an understanding of these combined phenomena to ensure that the proposed solutions will provide the desired level of protection in an efficient and cost effective manner.

Several studies have looked at the effects of explosions on concrete, including both experimental and numerical studies (Luccioni and Luege, 2006; Xu and Lu, 2006; Silva and Lu, 2009; Tai, Chu et al., 2011; Wang, Zhang et al., 2013; Zhao and Chen, 2013; Pantelides, Garfield et al., 2014). The finite elements procedures generally could reproduce experimental results acceptably.

The impact phenomenon has also been considered in the past. Most of the studies concentrated on relatively large projectiles travelling at speeds below 500 m/s. These included experimental studies (Kojima, 1991; Ohno, Uchida et al., 1992), analytical solutions (Luk and Forrestal, 1987; Xu, Keer et al., 1997; Jones, Hughes et al., 2003; Li and Chen, 2003) and FEA studies, which managed to replicate experimental results (Hanchak, Forrestal et al., 1992; Wang, Li et al., 2007; Ranjan, Banerjee et al., 2014). As mentioned above, these works concentrated on lower speed projectiles and tended therefore to ignore effects such as the erosion of the steel material, which might instead affect the results significantly in the problem considered here. Forrestal, Frew et al. (1996) produced test results with impactor speeds of about 1000 m/s, showing that already at these velocities the projectile will be significantly deformed. Their results, together with others, have been extensively used to produce analytical methods to account for this effect. For example, Luk and Piekutowski (1991) produced a model which accounted for the elasto-plastic nature of the projectile, with several authors developing this approach further (Yaziv and Riegel, 1993; Roisman, Yarin et al., 2001; Rubin and Yarin, 2002). Khoda-rahmi, Fallahi et al. (2006) and Zhao, Chen et al. (2010) originated a different model for concrete penetration considering the effects of projectile erosion employing a step process, where the penetration depth and the erosion were calculated alternatively. However, there are not many FEA studies available for high speed deforming projectiles into concrete. Some such studies have been performed for other materials, such as fabrics (Barauskas and Abraitienė, 2007), where it was shown that relatively simple elasto-plastic models can handle the severe deformations of the projectile.

Fewer studies are available for the combined effects of impacts and blast loading. Hader (Hader, 1983) during his tests did find that cased charges produced significantly more damage than uncased ones. More recently, Forsén and Nordström (Forsén and Nordström, 1992; Nordström, Forsén et al., 1994) conducted several experiments loading slabs resting on the ground with fragments and blast pressures. Similarly to this study, the fragments were represented with ball bearings, in their case 4 mm in diameter. The specimens were then tested statically and their energy absorption capacity was measured. This was then related to the density of fragments hitting the slab. Leppänen (2005) produced both experimental data and a numerical model of fragments and blast wave loading on a mass concrete element. The finite element model was produced using AUTODYN with a Lagrangian formulation and using the RHT material model for the concrete (Riedel, Thoma et al., 1999; Riedel, 2009). After the tests the authors produced sections of the samples showing the cracking pattern for comparison with the numerical results. The same author (Leppänen, 2006) also performed a detailed analysis of an impact employing the same RHT material model with a smooth

particle hydrodynamics (SPH) formulation. Accurate results were produced by the simulation. More recently, Nyström and Gylltoft (2009) also carried out a numerical study on this topic, this time considering reinforced concrete walls. They used a similar method, with the same concrete material model as used by previous authors. However, in this case reinforcement was included using beam elements and a rate sensitive Johnson Cook formulation.

Therefore, whilst the individual impact and blast events have been studied extensively, their combined effect is the object of far fewer experimental and numerical studies. Recently, experiments have been performed on slabs subject to the combined loads by placing ball bearings on an explosive charge so as to produce high velocity debris which would impact the slab. In this study the results from the dynamic portion of these experiments has been simulated numerically using LS-DYNA. The simulations attempted to include both the effects of the high velocity ball bearing projectiles and of the blast waves, comparing the damage produced to the images from the experimental programme and an analytical solution for the penetration depth.

2 METHOD

2.1 Experimental Program

The experiments were performed by the Defence Science and Technology Agency (DSTA) of Singapore in collaboration with the FOI, Swedish Defence Research Agency. Several concrete targets were used. All slabs were 1.6 m x 0.8 m in planar dimension. Their thickness was varied between 100 and 200 mm. The top reinforcement cover was 20 mm, whilst the bottom cover was 16 mm. The reinforcing bars were made with grade 500 deformed steel. All were 6 mm diameter. The transverse bars were always 200 mm centre to centre. The longitudinal bars spacing was either twelve bars at 75 mm centre to centre or six bars at 150 mm centre to centre for each thickness used. Therefore, four slab geometries were tested in total. The concrete grade was measured with cube tests after the experiments and varied between $f_{cu} = 36.6$ MPa and $f_{cu} = 38.1$ MPa. All slabs were placed on sand bedding directly underneath the charge.

In all cases the charges were located above the centre of the slab with a stand-off of 2.1 m. The explosive weights varied between 8.883 and 8.93kg of TNT. The charges were cylinders 200 mm in diameter and height, with the bottom surface shaped as a 200 mm radius sphere. Approximately 346 steel ball bearings 8 mm in diameter were placed underneath the explosive on the spherical surface to simulate the fragments impact from a real charge. A typical test set up is shown in Figure 1, which shows the slab and the charge above it.

High speed photography was employed to measure the ball bearings speed near the slab surface. Photographs of the slabs tops were taken after the test to identify impact points and the degree of damage caused by the loading. Additionally, measurements of the penetration depths of the fragments were taken on site and crater sizes were measured from the experimental images.

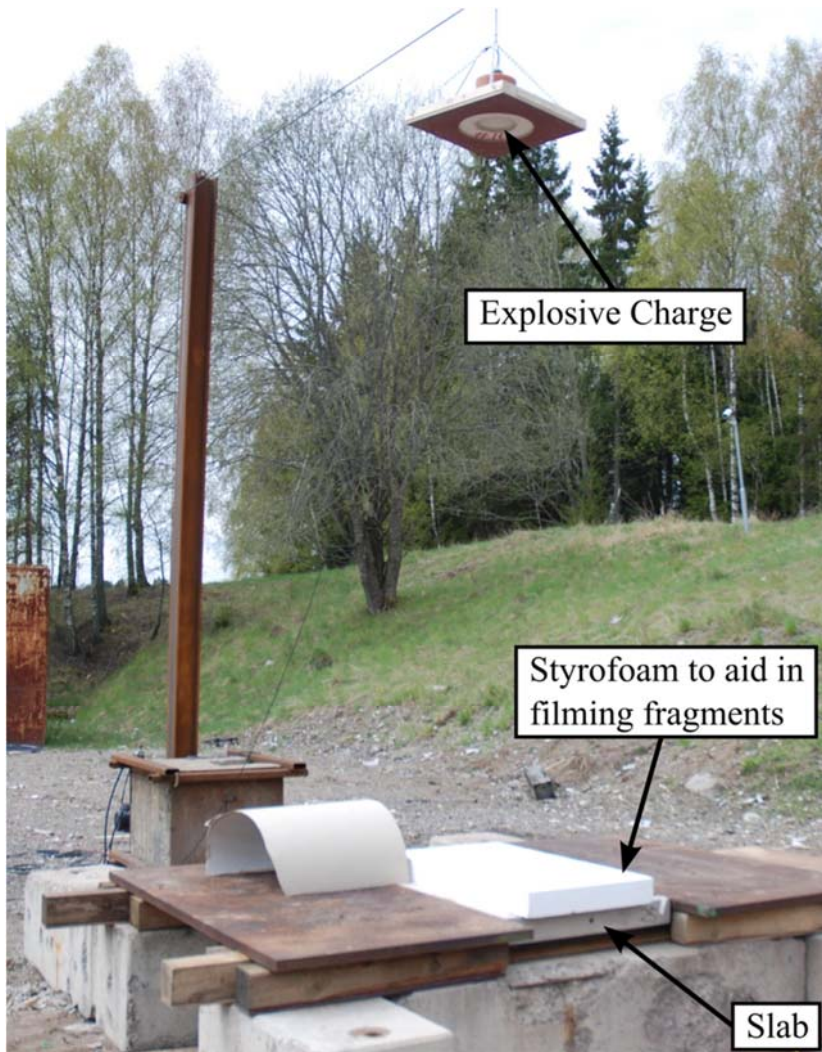


Figure 1: Experimental set up used in the tests. The image was provided by and is the property of DSTA.

2.2 Analytical Solution for Penetration Depth

As only final damage images and approximate penetration depth information were available for comparison with FEA, an additional penetration depth calculation was performed using the method proposed by Xu, Keer et al. (1997) for elastic-cracked materials. This was chosen as the reinforcement concentration used in the experiments was low and the projectiles only penetrated the concrete surface. Therefore a brittle model was likely to be more accurate than the plastic model derived by Luk and Forrestal (1987). For the calculation, it was assumed that $\eta=0.1$ and the Concrete Young's modulus was calculated using the rate dependency method proposed in the CEB FIP 1990 code (Comite Euro-International Du Beton, 1993), using the equation:

$$\frac{E_{c,imp}}{E_{ci}} = \left(\frac{\dot{\epsilon}_c}{\dot{\epsilon}_{co}} \right)^{0.026} \quad (1)$$

Where $E_{c,imp}$ is the high rate Young's modulus, $\dot{\epsilon}_{co}$ is $-30 \times 10^{-6} \text{ s}^{-1}$, $\dot{\epsilon}_c$ is the strained rate assumed for the calculation and E_{ci} was taken as $35 \times 10^3 \text{ MPa}$, assuming a concrete grade between C40 and C30 and using table 2.1.6 in the code.

The concrete density was taken as 2400 kg/m^3 , the projectile speed was assumed to be 1780 m/s and the ball bearings dimensions were used when calculating the projectile mass. For the calculation, it was assumed the projectile hit the slab surface vertically. The penetration depth obtained could then be compared with the results from the finite element simulation.

2.3 Finite Element Simulation

The models were used to simulate both the fragment and the blast wave impact on the slabs. LS-Dyna was used to produce the model. The software had been used previously by several authors studying reinforced concrete structures, both for projectile (Wang, Li et al., 2007) and for vehicle impact (Zain and Mohammed, 2015). As the size of the model was large, and producing a relatively rapid procedure to produce damage estimates was a requirement of the project, it was decided to use a Lagrangian formulation instead of Eulerian or SPH formations used in the past by others authors (Leppänen, 2006). The two loading phenomena differ significantly both in terms of the typology of the damage likely to be inflicted and on the time period of the load applications and the duration of its effect. The fragments were modelled as impacting at very high speed, approximately 1750 m/s . At this speed the steel fragments will be damaged and the entire impact event will be concluded within 5×10^{-5} seconds. Instead, the blast wave loading itself might last longer than a millisecond and the induced vibrations in the slab will occupy a significantly longer time period to dissipate. Additionally, the mesh size for the spherical bearings proved to be very important and needed to be finer than the size used in other parts of the model. Due to this, the stable time increments determined by the impactors were significantly smaller than those of the reinforced concrete slab parts. Whilst these short steps proved acceptable to model the timescales of interest for the impact analysis, the significantly longer period required by the blast analysis proved impracticable to run with the same model characteristics. It was therefore decided to split the analysis in two sections. Firstly the impact analysis was run for 5×10^{-5} seconds. A restart analysis was then run including the blast wave arrival and subsequent structural response. In this second analysis the remaining fragments of the ball bearings were eliminated to ensure the stable time steps were of sufficient size to guarantee a practical computing time. This second analysis was run for a period of 10 ms , after which the dynamic effects became less important.

The FEA geometry mirrored the slabs used in the tests, representing all four slab types in separate models. Solid hexahedral elements were used for the concrete, whilst beam 1D truss elements were used for the reinforcement mesh. The reinforcement planar distribution in the two cases is shown in Figure 2. The top and bottom covers were 20 mm and 16 mm respectively as in the experimental specimens. A 2 mm mesh size was used in plan throughout the models. The thickness element dimension was gradually varied from a minimum of 2 mm in the area above the top reinforcement to about 10 mm at the bottom of the slab. The K&C revision 3 material model (MAT_72R3) (Malvar, Crawford et al., 1997; Crawford and Malvar, 2006; Hallquist, 2007) was used to model the concrete. This material model was used in the past by others for blast simula-

tions (Wang, Zhang et al., 2013; Zhao and Chen, 2013). Whilst some authors use different material models, for example the CSCM model (Ranjan, Banerjee et al., 2014), in this case the K&C model was found to produce more accurate results, possibly due to the significantly higher impact velocities considered. No information on the characteristics of the concrete mix used in the experiments was provided, with the exception of the cube strength which had been measured with laboratory tests on the material used for the experimental samples. Therefore, it was decided to employ the automatic parameter generation function for the appropriate values of concrete cylinder strength. The concrete material model required the input of a curve to define the dynamic increase factor (DIF) of the material capacity at different rates. The software would then interpolate between the given values. The curve was derived using the functions given by Malvar and Ross (1998) for tension and the CEB FIP 1990 code (Comite Euro-International Du Beton, 1993) for compression. The tension function was:

$$\begin{aligned} \frac{f_t}{f_{ts}} &= \left(\frac{\dot{\epsilon}}{\dot{\epsilon}_s} \right)^\delta \quad \text{for } \dot{\epsilon} \leq 1 \text{ s}^{-1} \\ \frac{f_t}{f_{ts}} &= \beta \left(\frac{\dot{\epsilon}}{\dot{\epsilon}_s} \right)^{1/3} \quad \text{for } \dot{\epsilon} > 1 \text{ s}^{-1} \end{aligned} \tag{2}$$

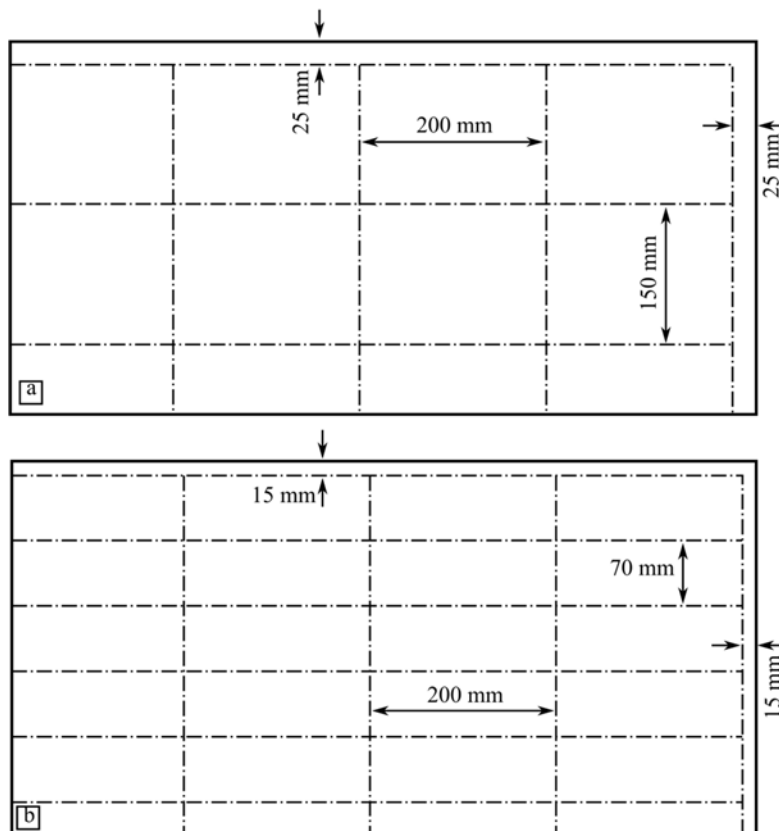


Figure 2: Reinforcement distribution on the quarter of the slab included in the FEA models.

Where f_t was the dynamic tensile strength at strain rate $\dot{\epsilon}$, f_{ts} was the dynamic tensile strength at strain rate $\dot{\epsilon}_s = 10^{-6} \text{ s}^{-1}$, f_t/f_{ts} was the tensile (DIF) used for the material model, δ was given by $\delta = 1/(1 + 8 f'_c/f'_{co})$, f'_{co} was 10 MPa and f'_c was the cylinder compressive strength of the concrete material and $\log \beta = 6\delta - 2$. The compression function was:

$$\begin{aligned} f_c/f_{cs} &= \left(\frac{\dot{\epsilon}}{\dot{\epsilon}_{sc}} \right)^{1.026\delta_c} & \text{for } \dot{\epsilon} \leq 30 \text{ s}^{-1} \\ f_c/f_{cs} &= \gamma \left(\frac{\dot{\epsilon}}{\dot{\epsilon}_{sc}} \right)^{1/3} & \text{for } \dot{\epsilon} > 30 \text{ s}^{-1} \end{aligned} \quad (3)$$

Where f_c was the dynamic tensile strength at strain rate $\dot{\epsilon}$, f_{cs} was the dynamic tensile strength at strain rate $\dot{\epsilon}_{sc} = 30 \times 10^{-6} \text{ s}^{-1}$, f_c/f_{cs} was the compressive DIF, δ was given by $\delta_c = 1/(5 + 9 f'_c/f'_{co})$ and $\log \gamma = 6.15\delta_c - 2$. As the formulae show, the DIC was dependent on the concrete grade. However, as the results for the strengths to be used varied by less than 1% from a mean value, a curve for 37.5 MPa f_{ck} was used. Erosion was used to simulate the damage and avoid convergence issues in the model. Principal strain was used for this, with a maximum limit of 1.0 and a minimum (tension) limit of 0.2. These limits were chosen to be high enough to ensure no effect on the damage distributions, whilst avoiding convergence issues, and were determined following a parametric study on the FEA models. The steel reinforcement was treated as elastic-perfectly plastic, with an elastic stiffness of 200 GPa, a Poisson ratio of 0.3 and a yield strength of 500 MPa.

The steel bearings were meshed with 1 mm hexahedral elements. In literature, when modelling concrete targets, the impactors have been represented either as rigid (Wang, Li et al., 2007) or deformable elasto-plastic materials with or without strain rate effects (Raguraman, Deb et al., 2008; Liu, Huang et al., 2011; Ranjan, Banerjee et al., 2014). As the deformation of these components was an important parameter of the analysis, it was decided to include this factor in the models. To ensure the strain rate and plastic deformations would be modelled appropriately, a Johnson-Cook material was applied. The simplified model provided in LS-DYNA (MAT_098) (Hallquist, 2007) was used. The steel grade AISI 52100 was assumed for all the ball bearings. The material parameters for this grade were obtained from Shrot and Bäker (2012) and were included in the model with an erosion limit of 20%.

Symmetry boundary conditions were introduced on two of the sides, as only a quarter of the slab was included in the model. The bottom of the slab was pinned since no bouncing was observed in high speed videos during the tests.

Real impact locations as found in the experimental images were used in the FEA models, leading to between 12 and 21 ball bearings impacting the quarter slabs in the model. A straight path from the charge was assumed to estimate a travel direction for each fragment, introducing therefore some horizontal components in the velocities which varied between 1650 m/s and 1780 m/s. Whilst the blast loads could have been simulated using Eulerian approaches (Trajkovski, Kunc et al., 2014), in this case it was decided to use the CONWEP module built into LS-DYNA. This allowed

for the pressure intensity and exact arrival time to be varied on the slab surface in a realistic manner.

The FEA results were compared both with the analytical solution and with the experimental results. The main output and source of comparison data was the damage distribution, as the experimental configuration with the slab on the ground prevented the collection of more global data, such as deflections and reaction forces. Instead, a typical impact at an isolated location was chosen and the penetration depth and crater size were measured. These data could then be compared with the experimental measurements and analytical calculations for these values.

After the detailed results were assessed, the overall damage on the top slab surface could be compared with the experimental images.

3 RESULTS

3.1 Experimental Results

The slabs were subjected to the blast and impact loading as described above. The fragments velocities were measured and images were taken of the top slab surfaces to record the impact locations and damage extent.

The fragment velocities measured ranged from 1650 m/s and 1780 m/s as mentioned in the FEA description. At these speeds the fragments underwent significant deformation on impact, which is likely to have affected the damage extent on the slabs. Typical slab damage is shown in Figure 3. In all cases damage craters varied in size between approximately 50 mm and 120 mm diameter, with most isolated craters between 50 and 70 mm as shown in Figure 4, and the penetration holes were between 20 and 25 mm deep. The damage was more widespread near the edges of the slab, where the corner section spalled off in some instances. Some hairline cracks connected the craters, however it was reported that the samples were still able to be lifted in one piece, and no significant damage was observed on their underside. This indicates that the damage could be quite superficial and that significant capacity would still be available in the specimens. This damage information was used to assess the results from the FEA models.



Figure 3: Damage on the top surface of a 200 mm slab. This test was as a source for the impact locations in test 1 of the FEA simulations. The image was provided by and is the property of DSTA.

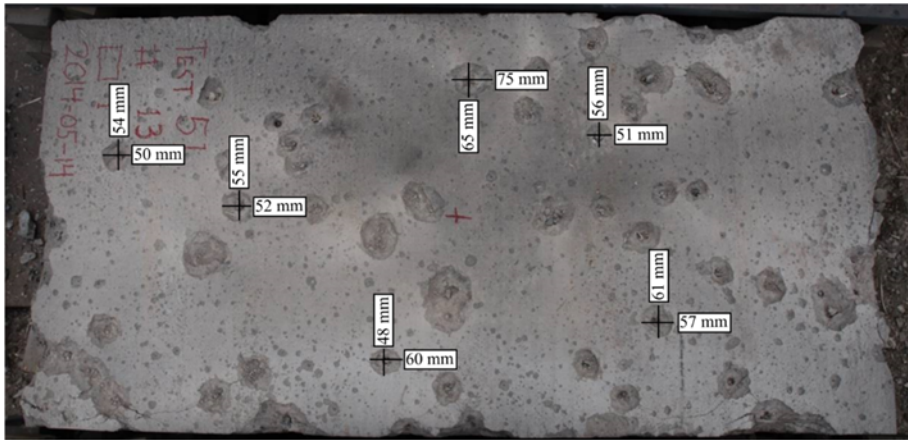


Figure 4: Typical isolated crater sizes on the slab surface. The test which provided locations for test 3 in the FEA simulations is shown. The original image was provided by and is the property of DSTA

3.2 Analytical

The analytical method presented above was used to calculate the expected penetration depth of fragments into the slab. Firstly, the Concrete Young's modulus was estimated using the strain rates measured in the FEA analysis. A typical result is shown in Figure 5. An average strain rate of 100000 s^{-1} was assumed, producing a Young's modulus of $62 \times 10^3 \text{ MPa}$ with equation 1. This was then used to calculate the penetration depth, which was found to be 20.2 mm. The result is therefore compatible with the experimental measurements, though it is on the lower end of their range.

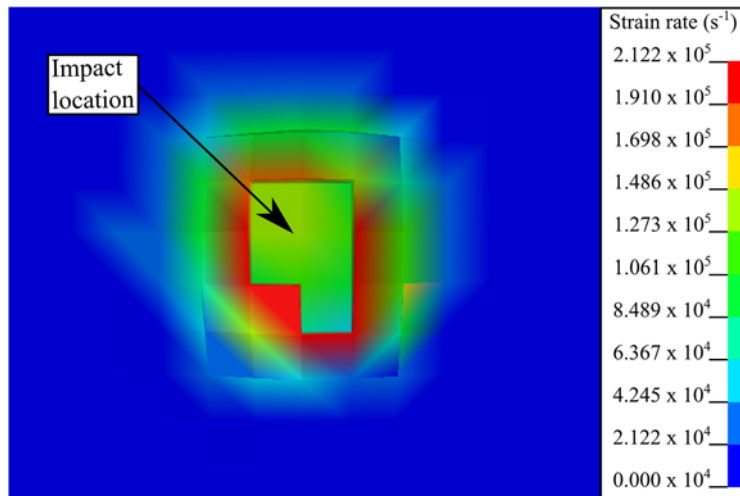


Figure 5: Typical strain rates in the concrete during impact.

3.3 FEA Results

The models were run using the speeds obtained from the experimental data as described above. The aim was to compare the simulated damage with the images available for the tests.

The initial 5×10^{-5} seconds impact simulation produced data on the initial penetration process and the depth reached by the projectiles. A time history of the penetration of one typical projectile is shown in Figure 6. In this time frame the damage is limited to the immediate vicinity of the impact, with some small evidence of light damage on the underside of the slab. The penetration depths were between 20 and 23 mm in all cases.

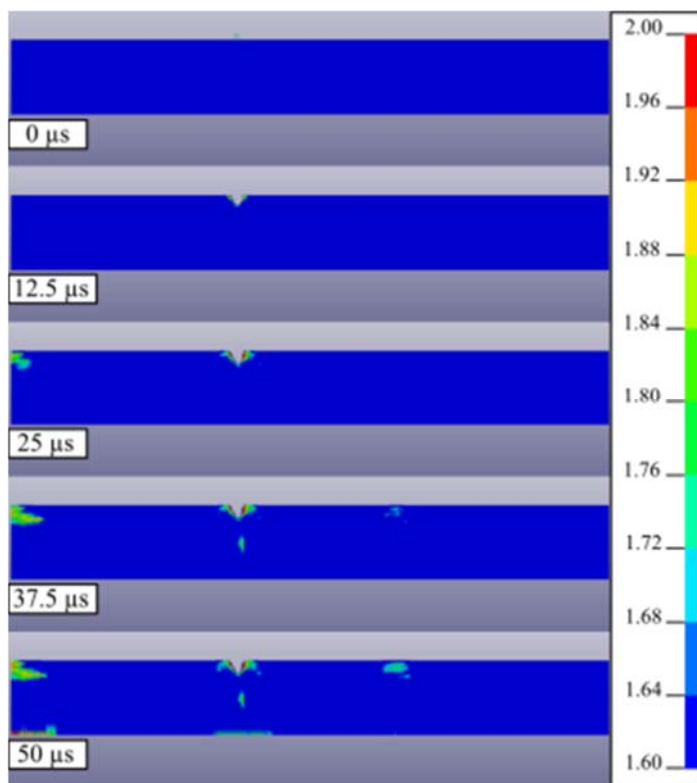


Figure 6: Sections of a 100 mm slab at an impact location taken at different time points showing the progressive damage to the impactor and the slab. Damage levels above 1.8 indicate probable cracking of the material.

The following 10 ms analyses produced more data on the final damage levels. Figure 7 shows the top of the slabs in the four cases. The damaged areas diameters are approximately 50 mm, and there is evidence of cracks connecting the impact locations. Additionally, more severe damage can be seen where several fragments impacted the slabs near their edges. The extent of cracks suggests that the area of concrete might spall. Figure 8 shows a cross section through an impact location, with the same damage scale as used in Figure 7. This shows that cracks spread underneath the surface, indicating that a wider area of concrete is damaged than obvious from the top surface images.

Detailed results for an isolated crater form test 2 are shown in Figure 9. The depth of the crater is 22 mm, whilst its radius is 62 mm maximum. Whilst the depth measurement could be made precisely, the radius of the crater was more subjective and was dependant on the interpretation of the material damage given by the model. The figure of 62 mm represents a maximum measurement, whilst the minimum, covering the damage reaching from the eroded hole to the surface, was 40 mm.

It is likely that the real crater size would therefore fall between these limits, as suggested by the 50 mm overall estimate previously made.

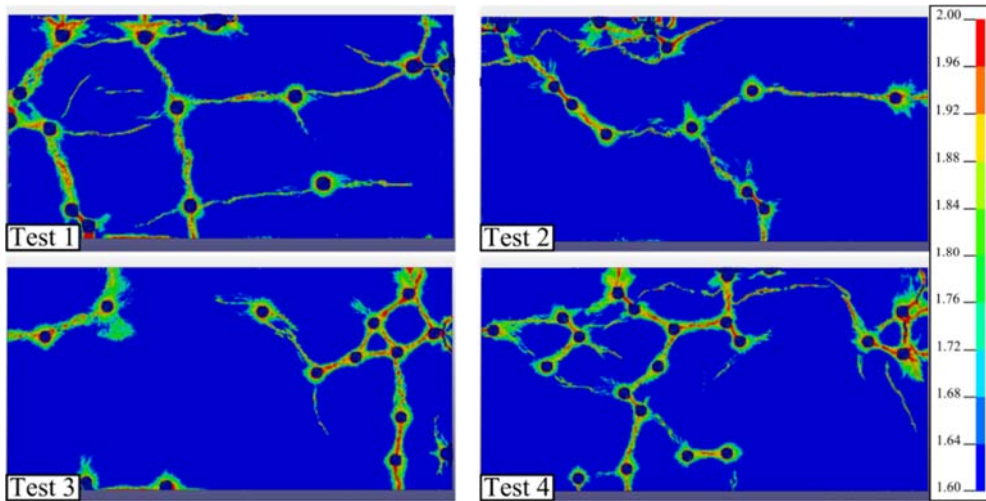


Figure 7: Top damage for the four tests at 10 ms. Material damage from 1.6 was shown to highlight areas more likely to have cracked.

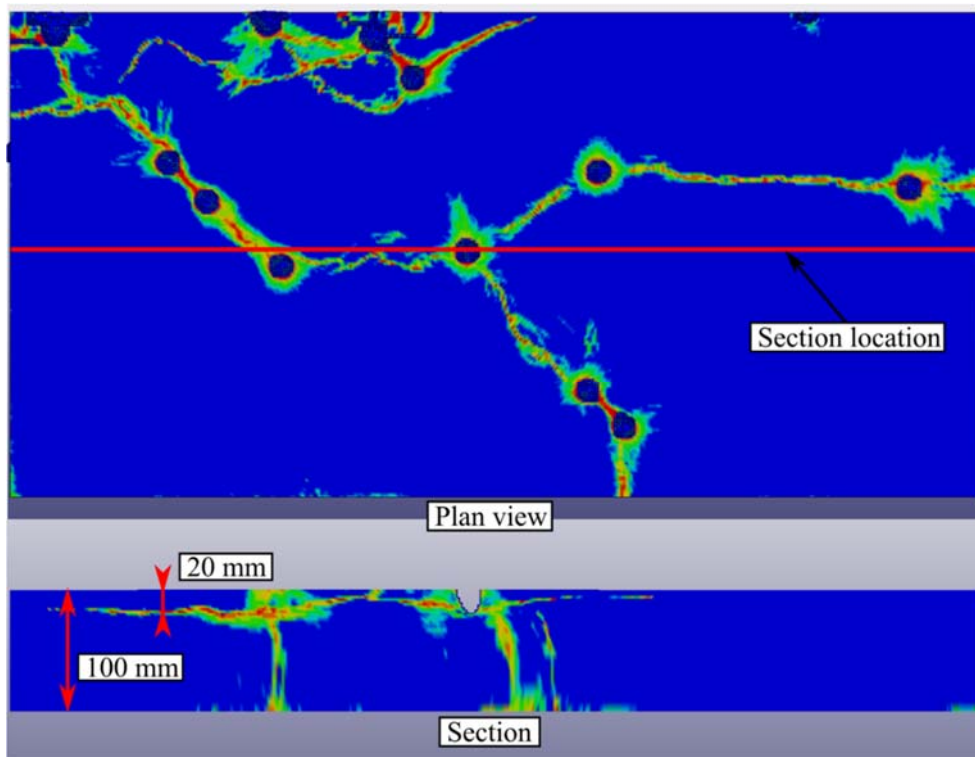


Figure 8: A section through the test 2 slab at an impactor location. Cracks running underneath the concrete surface can be seen. Material damage from 1.6 was shown to highlight areas more likely to have cracked.

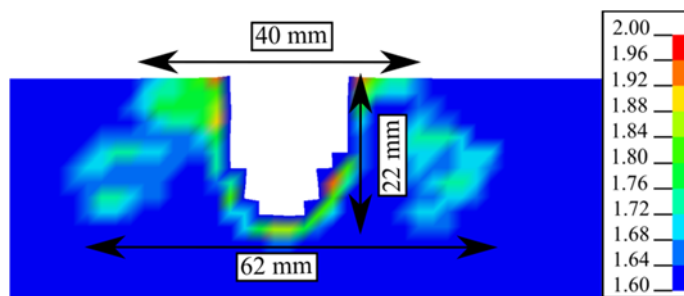


Figure 9: Detailed damage at an isolated impact location in test 2. The crater dimensions are shown. Material damage from 1.6 was shown to highlight areas more likely to have cracked.

4 ANALYSIS

FEA models were run to simulate the available experiments, with the aim of comparing the simulation results to the experimental data. Damage extent results were compared, as this was the main information available from the experimental program. The FEA results plots were always produced setting the colour scale to a minimum of 1.6. This was done to highlight the areas with a chance of cracking rather than earlier, partial damage occurrences which might not cause visible changes in the sample.

The detailed results at an isolated impact location were firstly compared to the analytical and experimental results. The penetration depths and crater size results are shown in Table 1. The results show that the FEA results were compatible to both the analytical and experimental values, though there was some variation in the measured results. This was especially true for the crater sizes, which varied significantly depending on the method adopted to measure their size. It is however likely that the crater size would have been between the two measured extremes, producing sizes of approximately 50 mm, comparable with the smaller sizes produced in the experiment. The variability of sizes was also present in the experiment, showing the strong dependence of the damage on factors which were not measured in the experiment, such as more detailed material properties.

Damage measure	Experimental results	Analytical solution	FEA results
Penetration Depth (mm)	20 - 25	20.2	20 - 22
Crater radius (mm)	50 - 70	N/A	40 - 62

Table 1: Isolated impact damage results.

The penetration depths instead agreed more closely. The analytical solution result is relatively low, especially as it assumed an impact velocity with no horizontal components. It should be noted that most analytical solutions for penetration in concrete have been derived for larger, generally rod impactors. Therefore, the spherical ball bearing case studied here was somewhat outside the derivation assumptions made by the authors. This was more strongly the case for deformable projectile analyses, such as the one produced by Luk and Piekutowski (1991), as in that case a large part of

the initial physical assumptions depended on the specific projectile shape. For this reason, whilst the measured velocities and experimental observations suggested that the projectile would deform and erode during impact, it was decided to utilise a rigid projectile solution for this analysis. The results though suggested that such a choice could produce reasonable results for the penetration depth of this kind of projectile.

Figure 10 and Figure 11 compare the top surface damage areas for various tests with the experimental images. Generally the top surface damage seems lower in the numerical simulation, especially in the case of test 1 and test 3. As mentioned previously though, significant damage could be seen in sections below the slab surface.

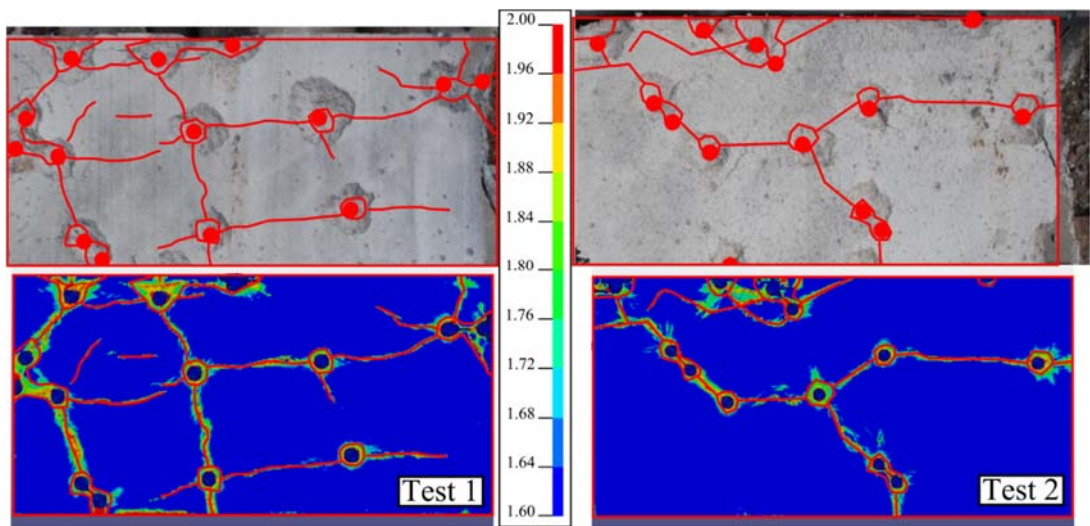


Figure 10: Comparison of superficial damage area for test 1 (left hand side) and test 2 (right hand side).

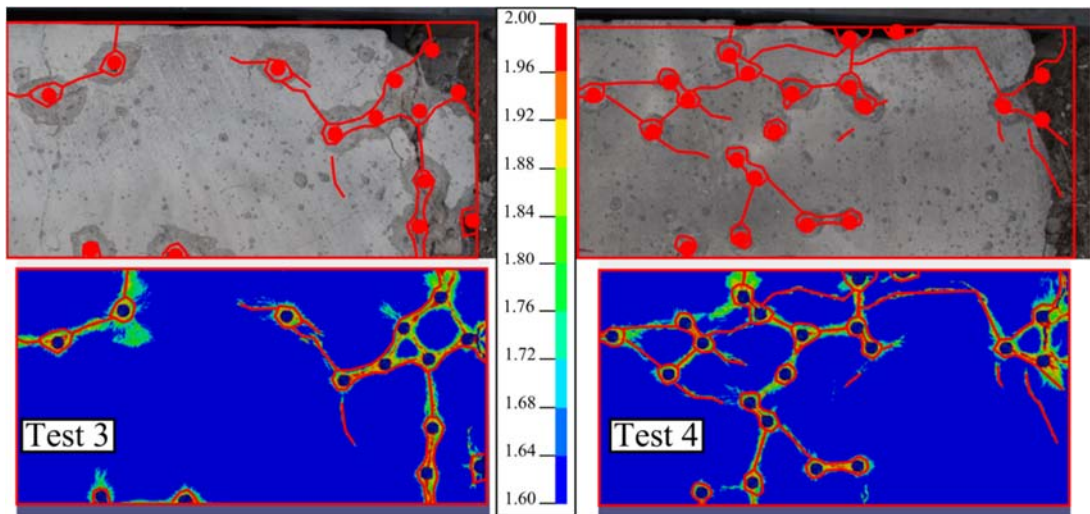


Figure 11: Comparison of superficial damage area for test 3 (left hand side) and test 4 (right hand side).

Figure 12 and Figure 13 show this with sections from the tests. This shows that the damage extent is generally significantly closer to the experiments than what was seen previously, and, especially for test 1, includes also some edge damage not evident in the top surface plot. However, in the other cases, and especially for test 4, the simulated damage was larger than what could be seen in the available image. This difference could be due to discrepancies in the slab materials and impact characteristics. This would have limited the damage to the areas directly near the penetration holes, which are similar to those seen in the top surface view of the FEA results. These results therefore showed that the FEA models were able to reasonably predict the damage inflicted on a slab by this complex loading. However, the damage could only be compared with images of the top surface of the slabs. Further information might be used in future stages of the project, enabling a more qualitative comparison to be performed.

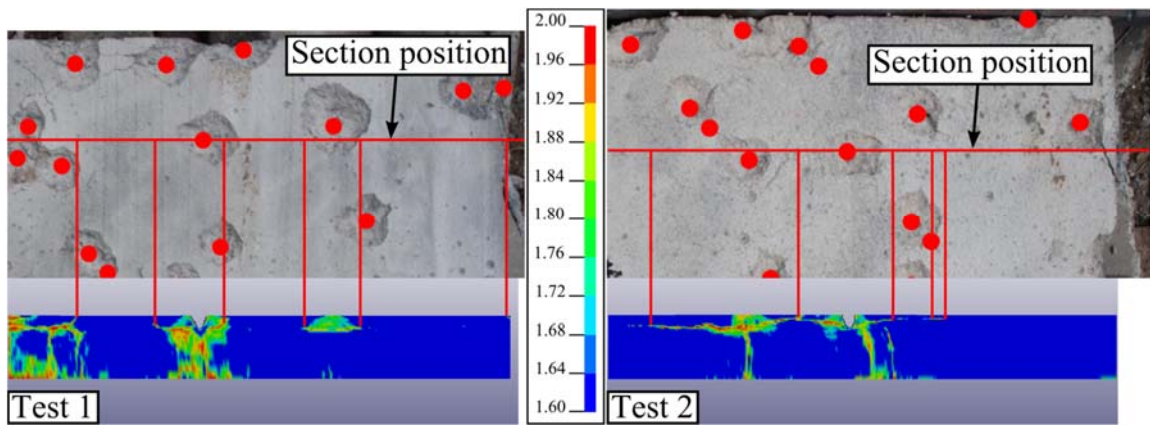


Figure 12: Section at an impact location compared to the images of the experimental damage for test 1 (left hand side) and test 2 (right hand side).

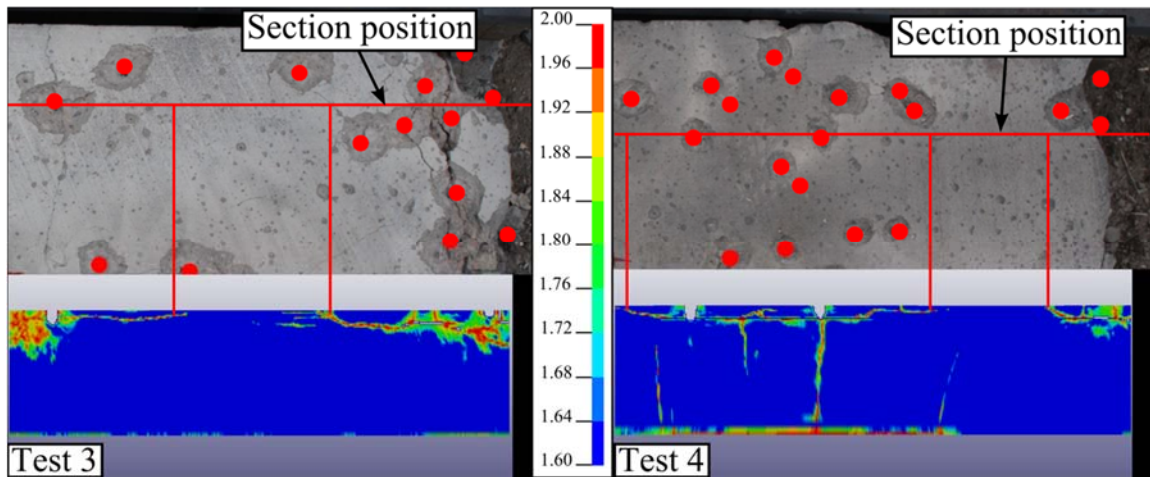


Figure 13: Section at an impact location compared to the images of the experimental damage for test 3 (left hand side) and test 4 (right hand side).

5 CONCLUSIONS

The performance of concrete slabs under combined impact and blast loading has been studied with the aim of producing a numerical simulation of the phenomena. Data from an experimental investigation of the problem were available, allowing for a comparison with numerical and analytical results.

FEA quarter models of the four combinations of slab thickness and reinforcement densities were created and loaded in accordance with the experimental information available. The typical penetration depth was also estimated with an analytical method. The exact level of agreement between the FEA and the experimental records varied between the different tests, however in general the results on the penetration depths of the impactors and the level of damage around the impact sites were realistic. The analytical solution results also agreed with the penetration depths measured from the experiment and numerical simulation. This represented a positive result, especially as little information was available on the characteristics of the material used, therefore showing that the automatically generated material parameters were sufficient to represent these phenomena acceptably.

Whilst the current results are promising, several further studies should be performed to expand and improve them. Firstly, further validation of the numerical results will be needed. Comparison with other records of the damage would be beneficial; however the most significant comparison will be between the static residual capacity data and the equivalent simulation to be run using the numerical results of this study. This will be the focus of the next phase of this project as it will conclusively determine the quality of the simulation.

It is hoped that the work presented here, together with the suggested improvements, will go towards being able to simulate these loading conditions and lead to safer, more economical design of structures.

Acknowledgments

This research was supported by a research grant provided by the Defence Science & Technology Agency (DSTA), Singapore, under the Protective Technology Research Centre, Nanyang Technological University, Singapore. Any opinions, findings and conclusions expressed in this presentation are those of the writers and do not necessarily reflect the view of DSTA, Singapore.

References

- Barauskas, R. and Abraitienė, A., (2007). Computational analysis of impact of a bullet against the multilayer fabrics in LS-DYNA, *International Journal of Impact Engineering* 34(7): 1286-1305.
- Comite Euro-International Du Beton, (1993). *Design of Concrete Structures*. CEB-FIP Model Code 1990, Thomas Telford (London).
- Crawford, J. E. and Malvar, L. J. (2006). TR-06-19.1: User's and theoretical manual for K&C concrete model. Burbank, CA.
- Forrestal, M. J., Frew, D. J., Hanchak, S. J. and Brar, N. S., (1996). Penetration of grout and concrete targets with ogive-nose steel projectiles, *International Journal of Impact Engineering* 18(5): 465-476.
- Forsén, R. and Nordström, M., (1992). Damage to reinforced concrete slabs due to the combination of blast and fragment loading, FOA report B 20101-2.6, Swedish Defence Research Agency (Tumba, Sweden).

- Hader, H., (1983). Effects of Bare and Cased Explosives Charges on Reinforced Concrete Walls, Symposium Proceedings, The Interaction of Non-Nuclear Munitions with Structures (U.S. Air Force Academy, Colorado), May 10-13, pp. 221-226.
- Hallquist, J.O., (2007). LS-DYNA keyword user's manual (Version 970), Livermore Software Technology Corporation (USA).
- Hanchak, S. J., Forrestal, M. J., Young, E. R. and Ehrigott, J. Q., (1992). Perforation of concrete slabs with 48 MPa (7 ksi) and 140 MPa (20 ksi) unconfined compressive strengths, *International Journal of Impact Engineering* 12(1): 1-7.
- Jones, S. E., Hughes, M. L., Toness, O. A. and Davis, R. N., (2003). A one-dimensional analysis of rigid-body penetration with high-speed friction, *Proceedings of the Institution of Mechanical Engineers, Part C: Journal of Mechanical Engineering Science* 217(4): 411-422.
- Khoda-rahmi, H., Fallahi, A. and Liaghat, G. H., (2006). Incremental deformation and penetration analysis of deformable projectile into semi-infinite target, *International Journal of Solids and Structures* 43(3-4): 569-582.
- Kojima, I., (1991). An experimental study on local behavior of reinforced concrete slabs to missile impact, *Nuclear Engineering and Design* 130(2): 121-132.
- Leppänen, J., (2005). Experiments and numerical analyses of blast and fragment impacts on concrete, *International Journal of Impact Engineering* 31(7): 843-860.
- Leppänen, J., (2006). Concrete subjected to projectile and fragment impacts: Modelling of crack softening and strain rate dependency in tension, *International Journal of Impact Engineering* 32(11): 1828-1841.
- Li, Q. M. and Chen, X. W., (2003). Dimensionless formulae for penetration depth of concrete target impacted by a non-deformable projectile, *International Journal of Impact Engineering* 28(1): 93-116.
- Liu, Y., Huang, F. and Ma, A., (2011). Numerical simulations of oblique penetration into reinforced concrete targets, *Computers & Mathematics with Applications* 61(8): 2168-2171.
- Luccioni, B. M. and Luege, M., (2006). Concrete pavement slab under blast loads, *International Journal of Impact Engineering* 32(8): 1248-1266.
- Luk, V. K. and Forrestal, M. J., (1987). Penetration into semi-infinite reinforced-concrete targets with spherical and ogival nose projectiles, *International Journal of Impact Engineering* 6(4): 291-301.
- Luk, V. K. and Piekutowski, A. J., (1991). An analytical model on penetration of eroding long rods into metallic targets, *International Journal of Impact Engineering* 11(3): 323-340.
- Malvar, L. J. and Ross, C. A., (1998). Review of Strain Rate Effects for Concrete in Tension, *ACI Materials Journal* 95(6): 735-739.
- Malvar, L. J., Crawford, J. E., Wesevich, J. W. and Simons, D., (1997). A plasticity concrete material model for DYNA3D, *International Journal of Impact Engineering* 19(9-10): 847-873.
- Nordström, M., Forsén, R. and Bulson, P. S. (1994). Damage to reinforced concrete slabs due to fragment loading with different fragment velocities, fragment areal densities and sizes of fragments. *Structures under Shock and Impact III*. Ashurst, Computational Mechanics Publications: 131-138.
- Nyström, U. and Gylltoft, K., (2009). Numerical studies of the combined effects of blast and fragment loading, *International Journal of Impact Engineering* 36(8): 995-1005.
- Ohno, T., Uchida, T., Matsumoto, N. and Takahashi, Y., (1992). Local damage of reinforced concrete slabs by impact of deformable projectiles, *Nuclear Engineering and Design* 138(1): 45-52.
- Pantelides, C. P., Garfield, T. T., Richins, W. D., Larson, T. K. and Blakeley, J. E., (2014). Reinforced concrete and fiber reinforced concrete panels subjected to blast detonations and post-blast static tests, *Engineering Structures* 76(0): 24-33.
- Raguraman, M., Deb, A. and Gupta, N., (2008). A simulation-driven study of oblique impact of ogival-nosed projectiles on mild steel armour plates, *Latin American Journal of Solids & Structures* 5(3).

- Ranjan, R., Banerjee, S., Singh, R. K. and Banerji, P., (2014). Local impact effects on concrete target due to missile: An empirical and numerical approach, *Annals of Nuclear Energy* 68: 262-275.
- Riedel, W. (2009). 10 Years RHT: A Review of Concrete Modelling and Hydrocode Applications. *Predictive Modeling of Dynamic Processes: A Tribute to Professor Klaus Thoma*. S. Hiermaier. Boston, MA, Springer US: 143-165.
- Riedel, W., Thoma, K., Hiermaier, S. and Schmolinske, E. (1999). Penetration of reinforced concrete by BETA-B-500 numerical analysis using a new macroscopic concrete model for hydrocodes. 9th Int Symp Interaction of the Effects of Munitions with Structures.
- Roisman, I. V., Yarin, A. L. and Rubin, M. B., (2001). Normal penetration of an eroding projectile into an elastic-plastic target, *International Journal of Impact Engineering* 25(6): 573-597.
- Rubin, M. B. and Yarin, A. L., (2002). A generalized formula for the penetration depth of a deformable projectile, *International Journal of Impact Engineering* 27(4): 387-398.
- Shrot, A. and Bäker, M., (2012). Determination of Johnson-Cook parameters from machining simulations, *Computational Materials Science* 52(1): 298-304.
- Silva, P. F. and Lu, B., (2009). Blast resistance capacity of reinforced concrete slabs, *Journal of Structural Engineering* VO - 135(6): 708-708.
- Tai, Y. S., Chu, T. L., Hu, H. T. and Wu, J. Y., (2011). Dynamic response of a reinforced concrete slab subjected to air blast load, *Theoretical and Applied Fracture Mechanics* 56(3): 140-147.
- Trajkovski, J., Kunc, R., Perenda, J. and Prebil, I., (2014). Minimum mesh design criteria for blast wave development and structural response - MMALE method, *Latin American Journal of Solids and Structures* 11: 1999-2017.
- Wang, W., Zhang, D., Lu, F., Wang, S.-c. and Tang, F., (2013). Experimental study and numerical simulation of the damage mode of a square reinforced concrete slab under close-in explosion, *Engineering Failure Analysis* 27: 41-51.
- Wang, Z.-l., Li, Y.-c., Shen, R. F. and Wang, J. G., (2007). Numerical study on craters and penetration of concrete slab by ogive-nose steel projectile, *Computers and Geotechnics* 34(1): 1-9.
- Xu, K. and Lu, Y., (2006). Numerical simulation study of spallation in reinforced concrete plates subjected to blast loading, *Computers & Structures* 84(5-6): 431-438.
- Xu, Y., Keer, L. M. and Luk, V. K., (1997). Elastic-cracked model for penetration into unreinforced concrete targets with ogival nose projectiles, *International Journal of Solids and Structures* 34(12): 1479-1491.
- Yaziv, D. and Riegel, J. P., (1993). The application of the integral theory of impact to model penetration of hypervelocity impact, *International Journal of Impact Engineering* 14(1-4): 843-850.
- Zain, M. F. B. M. and Mohammed, H. J., (2015). Concrete road barriers subjected to impact loads: An overview, *Latin American Journal of Solids and Structures* 12: 1824-1858.
- Zhao, C. F. and Chen, J. Y., (2013). Damage mechanism and mode of square reinforced concrete slab subjected to blast loading, *Theoretical and Applied Fracture Mechanics* 63-64: 54-62.
- Zhao, J., Chen, X. W., Jin, F. N. and Xu, Y., (2010). Depth of penetration of high-speed penetrator with including the effect of mass abrasion, *International Journal of Impact Engineering* 37(9): 971-979.